

# A Fast Explicit Operator Splitting Method for Passive Scalar Advection

Alina Chertock<sup>†</sup>, Charles R. Doering<sup>‡</sup>,  
Eugene Kashdan<sup>§</sup>, and Alexander Kurganov<sup>¶</sup>

## Abstract

The dispersal and mixing of scalar quantities such as concentrations or thermal energy are often modeled by advection-diffusion equations. Such problems arise in a wide variety of engineering, ecological and geophysical applications. In these situations a quantity such as chemical or pollutant concentration or temperature variation diffuses while being transported by the governing flow. In the passive scalar case, this flow prescribed and unaffected by the scalar. Both steady laminar and complex (chaotic, turbulent or random) time-dependent flows are of interest and such systems naturally lead to questions about the effectiveness of the stirring to disperse and mix the scalar. The development of reliable numerical methods for advection-diffusion equations is crucial for understanding their properties, both physical and mathematical. In this paper, we extend a fast explicit operator splitting method, recently proposed in [A. CHERTOCK, A. KURGANOV, AND G. PETROVA, *Internat. J. Numer. Meth. Fluids*, **59** (2009), pp. 309–332] for solving deterministic convection-diffusion equations, to the problems with random velocity fields and singular source terms. A superb performance of the method is demonstrated on several two-dimensional examples.

## 1 Introduction

Consider the inhomogeneous convection-diffusion equation

$$\rho_t + \nabla \cdot (\mathbf{u}\rho) = \kappa\Delta\rho + S(\mathbf{x}), \quad (1.1)$$

subject to the initial data

$$\rho(\mathbf{x}, 0) = \rho_0(\mathbf{x}), \quad (1.2)$$

where  $\rho(\mathbf{x}, t)$  is the concentration of a passive scalar field stirred by the divergence-free velocity  $\mathbf{u}(\mathbf{x}, t)$ , such that,  $\nabla \cdot \mathbf{u} = 0$  everywhere and at all times, and it is sustained by a steady source

---

<sup>†</sup>Department of Mathematics, North Carolina State University, Raleigh, NC 27695, USA; [chertock@math.ncsu.edu](mailto:chertock@math.ncsu.edu)

<sup>‡</sup>Departments of Mathematics & Physics, University of Michigan, Ann Arbor, MI 48109-1043, USA; [doering@umich.edu](mailto:doering@umich.edu)

<sup>§</sup>Department of Applied Mathematics, Tel Aviv University, Tel Aviv, Ramat Aviv, 69978, Israel; [ekashdan@post.tau.ac.il](mailto:ekashdan@post.tau.ac.il)

<sup>¶</sup>Department of Mathematics, Tulane University, New Orleans, LA 70118, USA; [kurganov@math.tulane.edu](mailto:kurganov@math.tulane.edu)

function  $S(\mathbf{x})$ . The positive constant  $\kappa$  in (1.1) is the molecular diffusivity. We restrict attention to the case without any net scalar flux at the boundary. In particular, equation (1.1) is studied on the periodic box of size  $L$ , that is,  $\mathbf{x} = (x_1, \dots, x_d) \in \mathbb{T}^d$  is the  $d$ -dimensional torus of volume  $L^d$ .

We are interested in fluctuations in the concentration  $\rho$  since the spatially averaged background density is irrelevant. We therefore change the variables to spatially mean-zero quantities

$$\theta(\mathbf{x}, t) = \rho(\mathbf{x}, t) - \frac{1}{L^d} \int_{\mathbb{T}^d} \rho(\mathbf{x}, t) d\mathbf{x} \quad \text{and} \quad s(\mathbf{x}) = S(\mathbf{x}) - \frac{1}{L^d} \int_{\mathbb{T}^d} S(\mathbf{x}) d\mathbf{x} \quad (1.3)$$

that satisfy the following initial-boundary value problem (IBVP):

$$\theta_t + \nabla \cdot (\mathbf{u}\theta) = \kappa\Delta\theta + s(\mathbf{x}), \quad \theta(\mathbf{x}, 0) = \theta_0(\mathbf{x}), \quad \theta \text{ is periodic.} \quad (1.4)$$

If  $\mathbf{u}$  is a given smooth velocity field and the source term  $s$  is nonsingular, the structure of the IBVP solution is quite simple, which makes it easy to design stable and convergent numerical methods for (1.4) (see, e.g., [7, 10, 19]). Obviously, in the convection-dominated regime ( $\kappa \ll 1$ ), a full resolution of “viscous shock layers” can be achieved only if the grid size is taken to be proportional to  $\kappa$ , which may be computationally unaffordable. Therefore, in practice, one is forced to use under-resolved methods, often stabilized by the excessive numerical viscosity, which, in turn, may badly affect the overall resolution. Another way to numerically preserve a necessary balance between convection, diffusion and source terms, is to use an operator splitting method, [16, 20, 21, 29, 31], briefly described in §2.

The IBVP (1.4) becomes much more difficult when the velocity field  $\mathbf{u}$  and/or the source term  $s$  are nonsmooth. In this paper, we study a single scaled flow with a temporally random velocity field and focus on singular (measure-valued) sources. In such a case, the IBVP (1.4) may be viewed as a “toy model” of turbulence (see [6, 28]), in which the solution is unstable and the only quantities one expects to capture numerically are time-space averaged *multi-scale mixing enhancement factors* introduced in [28] (see also §3 for details). In [28], the spectral method was used to compute the mixing enhancement factors in case of a random sine flow with smooth source terms. However, the spectral method is incapable to handle singular point-sources — the most interesting and challenging problem from the practical point of view.

To deal with singular sources, a particle method has been developed for the (1.1), (1.2) in [25]. The concentration field  $\rho$  was represented there by a distribution of particles, introduced by generating random locations with the properly normalized source  $S(\mathbf{x})$  as a probability distribution function. The particles are then transported by the advection  $\mathbf{u}$  and the diffusion, which is realized by adding independent Gaussian noises to  $\mathbf{u}$ . It should be observed, that a straightforward application of this method to (1.1), (1.2) will not produce reliable results due to statistical errors. Therefore, the implementation of particle method in [25] required a cumbersome algorithm of adding and removing particles during the computation, and its resolution is limited by the accuracy of the point values recovery procedure (see the discussion in [25]). In addition, a high computational cost of the particle method makes it difficult to extend the method to a more realistic model of turbulence, where the stirring velocity field  $\mathbf{u}$  is a turbulent solution of the incompressible Navier-Stokes equation.

In this paper, we propose an alternative approach for solving (1.4), which has straightforward implementation, and also is more accurate and robust than the spectral and particle methods

mentioned above. Our method, which is described in details in §2, is an extension of the *fast explicit operator splitting* method recently proposed in [1, 3, 4] (see also [2]).

The equation (1.4) is split into the hyperbolic,

$$\theta_t + \nabla \cdot (\mathbf{u}\theta) = 0, \tag{1.5}$$

and the parabolic,

$$\theta_t = \kappa\Delta\theta + s(\mathbf{x}), \tag{1.6}$$

equations. The hyperbolic equation (1.5) is solved by the second-order Godunov-type central-upwind scheme [15], which belongs to the class of simple, efficient, universal, and highly accurate methods for multidimensional hyperbolic conservation laws — central schemes (see [5, 12–14, 24, 27] and references therein). The parabolic equation (1.6) is solved using the exact solver implemented in the pseudo-spectral manner and the singular sources are naturally incorporated into it.

The next section includes a detailed discussion about the implementation of the fast explicit operator splitting method. The results of two-dimensional (2-D) numerical experiments are reported in §3, where we show that the proposed method can successfully treat the case of a random scaled flow with both smooth and singular sources as well as demonstrate the efficiency of the splitting technique in computing the multi-scale mixing enhancement coefficients. The summary and concluding remarks highlight the advantages of the presented approach compared to alternative numerical methods and give an insight into the generalization of this work to other challenging problems.

## 2 Description of the Numerical Method

We begin with a brief description of the operator splitting technique. Consider equation (1.4) and denote by  $\mathcal{S}_{\mathcal{H}}$  and  $\mathcal{S}_{\mathcal{P}}$  the *exact* solution operators associated with the corresponding hyperbolic, (1.5), and parabolic, (1.6), equations. Assume that the solution of the original convection-diffusion equation (1.4) is available at time  $t$ . Introduce a (small) time step  $\Delta t$  and evolve the solution of (1.4) from  $t$  to  $t + \Delta t$  in two substeps. First, the hyperbolic equation (1.5) is solved on the time interval  $(t, t + \Delta t]$ :

$$\theta^*(\mathbf{x}) = \mathcal{S}_{\mathcal{H}}(\Delta t)\theta(\mathbf{x}, t), \tag{2.1}$$

and then the parabolic solution operator is applied to  $\theta^*$ , yielding the following approximate solution at time  $t + \Delta t$ :

$$\theta(\mathbf{x}, t + \Delta t) = \mathcal{S}_{\mathcal{P}}(\Delta t)\theta^*(\mathbf{x}) = \mathcal{S}_{\mathcal{P}}(\Delta t)\mathcal{S}_{\mathcal{H}}(\Delta t)\theta(\mathbf{x}, t). \tag{2.2}$$

In general, if all solutions involved in the two-step splitting algorithm (2.1)–(2.2) are smooth, the operator splitting method is *first-order* accurate (see, e.g., [20, 21, 29]). Higher-order operator splitting algorithms can be derived by considering a larger number of substeps. For instance, one time step of the *second-order* Strang splitting method [20, 21, 29] consists of three substeps:

$$\theta(\mathbf{x}, t + \Delta t) = \mathcal{S}_{\mathcal{H}}(\Delta t/2)\mathcal{S}_{\mathcal{P}}(\Delta t)\mathcal{S}_{\mathcal{H}}(\Delta t/2)\theta(\mathbf{x}, t). \tag{2.3}$$

In computational simulations, the exact solution operators  $\mathcal{S}_{\mathcal{H}}$  and  $\mathcal{S}_{\mathcal{P}}$  are typically replaced by their numerical approximations. The hyperbolic, (1.5), and the parabolic, (1.6), subproblems,

which are of different nature, can be solved by different methods — this is one of the main advantages of the operator splitting technique. In [1, 3, 4], a new version of the splitting method, the fast explicit operator splitting method, was proposed (see also [2]). The two key components of this method are:

- A non-oscillatory shock-capturing hyperbolic solver (or, alternatively, a non-dissipative method of characteristics);
- The exact parabolic solver implemented using either the heat kernel solution formula or in the pseudo-spectral manner.

The major ingredient of the fast explicit operator splitting method is the exact parabolic solver, which is obviously unconditionally stable. Therefore, the splitting steps can be made arbitrarily large (in practice, the size of the splitting steps is restricted by the accuracy considerations and is typically proportional to the spatial mesh size). This is especially important when the source term  $s$  is singular, which makes the parabolic equation (1.6) extremely stiff.

The use of a finite-volume shock capturing hyperbolic solvers (see [5, 8, 11–15, 17, 24, 27]) allows one to accurately solve the inviscid equation (1.5). These methods are typically stable provided the CFL condition is satisfied. Therefore, if the splitting time step  $\Delta t$  is too large, a hyperbolic “substep” may consist of several hyperbolic evolution steps.

We now explain how the fast operating splitting method can be applied to the problem under consideration. Without loss of generality, we consider the IBVP (1.4) in two space dimensions:

$$\theta_t + (u\theta)_x + (u\theta)_y = \kappa\Delta\theta + s(x, y), \quad \theta(x, y, 0) = \theta_0(x, y), \quad \theta \text{ is periodic.} \quad (2.4)$$

The “hyperbolic” substep is carried out using the second-order semi-discrete central-upwind scheme [15], which belongs to the class of Godunov-type projection-evolution methods: the solution, approximated by a piecewise linear function, is evolved in time according to the integral form of the corresponding hyperbolic equation

$$\theta_t + (u\theta)_x + (u\theta)_y = 0.$$

We assume that the cell averages of the solution are computed over a uniform grid (the extension to the nonuniform Cartesian grids is quite straightforward),

$$\bar{\theta}_{j,k}(t) \approx \bar{\theta}(x_j, y_k, t) := \frac{1}{\Delta x \Delta y} \iint_{C_{j,k}} \theta(x, y, t) dx dy, \quad C_{j,k} := (x_{j-\frac{1}{2}}, x_{j+\frac{1}{2}}) \times (y_{k-\frac{1}{2}}, y_{k+\frac{1}{2}}),$$

and they are available at some time level  $t$  (here,  $\Delta x = x_{j+\frac{1}{2}} - x_{j-\frac{1}{2}}$  and  $\Delta y = y_{k+\frac{1}{2}} - y_{k-\frac{1}{2}}$  are small spatial scales). Then we use these cell averages to reconstruct a conservative second-order piecewise linear interpolant:

$$\tilde{\theta}(x, y; t) = \bar{\theta}_{j,k}(t) + (\theta_x)_{j,k}(x - x_j) + (\theta_y)_{j,k}(y - y_k) \quad \text{for } (x, y) \in C_{j,k}, \quad (2.5)$$

where the slopes  $(\theta_x)_{j,k}$  and  $(\theta_y)_{j,k}$  are (at least) first-order approximations of the partial derivatives  $\theta_x(x_j, y_k, t)$  and  $\theta_y(x_j, y_k, t)$ , respectively. In order to ensure a non-oscillatory nature of the reconstruction (which is a necessary condition for the overall scheme to be non-oscillatory), the

slopes should be computed using a nonlinear limiter. In the numerical experiments reported in §3, we have implemented a so-called *MinMod2* limiter (see, e.g., [18, 24, 30]):

$$(\theta_x)_{j,k} = \text{minmod} \left( 2 \frac{\bar{\theta}_{j+1,k}(t) - \bar{\theta}_{j,k}(t)}{\Delta x}, \frac{\bar{\theta}_{j+1,k}(t) - \bar{\theta}_{j-1,k}(t)}{2\Delta x}, 2 \frac{\bar{\theta}_{j,k}(t) - \bar{\theta}_{j-1,k}(t)}{\Delta x} \right), \quad (2.6)$$

$$(\theta_y)_{j,k} = \text{minmod} \left( 2 \frac{\bar{\theta}_{j,k+1}(t) - \bar{\theta}_{j,k}(t)}{\Delta y}, \frac{\bar{\theta}_{j,k+1}(t) - \bar{\theta}_{j,k-1}(t)}{2\Delta y}, 2 \frac{\bar{\theta}_{j,k}(t) - \bar{\theta}_{j,k-1}(t)}{\Delta y} \right), \quad (2.7)$$

where the multivariate minmod function is defined by

$$\text{minmod}(z_1, z_2, \dots) := \begin{cases} \min_j \{z_j\}, & \text{if } z_j > 0 \quad \forall j, \\ \max_j \{z_j\}, & \text{if } z_j < 0 \quad \forall j, \\ 0, & \text{otherwise.} \end{cases}$$

According to the central-upwind scheme from [15], the cell averages of  $\theta$  are evolved in time by solving the following system of time-dependent ODEs:

$$\frac{d}{dt} \bar{\theta}_{j,k}(t) = - \frac{H_{j+\frac{1}{2},k}^x(t) - H_{j-\frac{1}{2},k}^x(t)}{\Delta x} - \frac{H_{j,k+\frac{1}{2}}^y(t) - H_{j,k-\frac{1}{2}}^y(t)}{\Delta y}, \quad (2.8)$$

where  $H_{j+\frac{1}{2},k}^x(t)$  and  $H_{j,k+\frac{1}{2}}^y(t)$  are the central-upwind numerical fluxes

$$\begin{aligned} H_{j+\frac{1}{2},k}^x(t) &= \frac{a_{j+\frac{1}{2},k}^+ f(\theta_{j,k}^E) - a_{j+\frac{1}{2},k}^- f(\theta_{j+1,k}^W)}{a_{j+\frac{1}{2},k}^+ - a_{j+\frac{1}{2},k}^-} + \frac{a_{j+\frac{1}{2},k}^+ a_{j+\frac{1}{2},k}^-}{a_{j+\frac{1}{2},k}^+ - a_{j+\frac{1}{2},k}^-} [\theta_{j+1,k}^W - \theta_{j,k}^E], \\ H_{j,k+\frac{1}{2}}^y(t) &= \frac{b_{j,k+\frac{1}{2}}^+ g(\theta_{j,k}^N) - b_{j,k+\frac{1}{2}}^- g(\theta_{j,k+1}^S)}{b_{j,k+\frac{1}{2}}^+ - b_{j,k+\frac{1}{2}}^-} + \frac{b_{j,k+\frac{1}{2}}^+ b_{j,k+\frac{1}{2}}^-}{b_{j,k+\frac{1}{2}}^+ - b_{j,k+\frac{1}{2}}^-} [\theta_{j,k+1}^S - \theta_{j,k}^N]. \end{aligned} \quad (2.9)$$

Here  $f(\theta) := (u\theta)$ ,  $g(\theta) := (v\theta)$ , and  $\theta_{j,k}^{E,W,N,S}$  are the point values of a piecewise linear reconstruction (2.5):

$$\theta_{j,k}^E = \tilde{\theta}(x_{j+\frac{1}{2}}, y_k; t), \quad \theta_{j,k}^W = \tilde{\theta}(x_{j-\frac{1}{2}}, y_k; t), \quad \theta_{j,k}^N = \tilde{\theta}(x_j, y_{k+\frac{1}{2}}; t), \quad \theta_{j,k}^S = \tilde{\theta}(x_j, y_{k-\frac{1}{2}}; t).$$

Finally, the local one-sided propagation speeds can be approximated by

$$\begin{aligned} a_{j+\frac{1}{2},k}^+ &= \max \left\{ \sup_{(x,y) \in B_{j+\frac{1}{2},k}} u(x, y; t), 0 \right\}, & a_{j+\frac{1}{2},k}^- &= \min \left\{ \inf_{(x,y) \in B_{j+\frac{1}{2},k}} u(x, y; t), 0 \right\}, \\ b_{j,k+\frac{1}{2}}^+ &= \max \left\{ \sup_{(x,y) \in B_{j,k+\frac{1}{2}}} v(x, y; t), 0 \right\}, & b_{j,k+\frac{1}{2}}^- &= \min \left\{ \sup_{(x,y) \in B_{j,k+\frac{1}{2}}} v(x, y; t), 0 \right\}, \end{aligned}$$

where  $B_{j+\frac{1}{2},k}$  and  $B_{j,k+\frac{1}{2}}$  are small balls centered at  $(x_{j+\frac{1}{2}}, y_k)$  and  $(x_j, y_{k+\frac{1}{2}})$ , respectively. If the velocities  $u$  and  $v$  are continuous at these points, the above speeds can be approximated by

$$\begin{aligned} a_{j+\frac{1}{2},k}^+ &= \max \left\{ u(x_{j+\frac{1}{2}}, y_k; t), 0 \right\}, & a_{j+\frac{1}{2},k}^- &= \min \left\{ u(x_{j+\frac{1}{2}}, y_k; t), 0 \right\}, \\ b_{j,k+\frac{1}{2}}^+ &= \max \left\{ v(x_j, y_{k+\frac{1}{2}}; t), 0 \right\}, & b_{j,k+\frac{1}{2}}^- &= \min \left\{ v(x_j, y_{k+\frac{1}{2}}; t), 0 \right\}. \end{aligned} \quad (2.10)$$

In such a case, the central-upwind fluxes (2.9) reduce to much simpler upwind fluxes:

$$H_{j+\frac{1}{2},k}^x(t) = \begin{cases} u(x_{j+\frac{1}{2}}, y_k; t) \theta_{j,k}^E, & \text{if } u(x_{j+\frac{1}{2}}, y_k; t) > 0, \\ u(x_{j+\frac{1}{2}}, y_k; t) \theta_{j+1,k}^W, & \text{if } u(x_{j+\frac{1}{2}}, y_k; t) < 0, \end{cases} \quad (2.11)$$

$$H_{j,k+\frac{1}{2}}^y(t) = \begin{cases} v(x_j, y_{k+\frac{1}{2}}; t) \theta_{j,k}^N, & \text{if } v(x_j, y_{k+\frac{1}{2}}; t) > 0, \\ v(x_j, y_{k+\frac{1}{2}}; t) \theta_{j,k+1}^S, & \text{if } v(x_j, y_{k+\frac{1}{2}}; t) < 0. \end{cases} \quad (2.12)$$

Note that  $\theta_{j,k}^{E,W,N,S}$ ,  $a_{j+\frac{1}{2},k}^\pm$ , and  $b_{j,k+\frac{1}{2}}^\pm$  depend on  $t$ , but we suppress this dependence in formulae (2.9)–(2.12) to simplify the notation.

The system of ODEs (2.8) should be solved by a stable and accurate numerical method. In the reported numerical experiments, we have used the third-order strong stability preserving (SSP) Runge-Kutta solver [9].

Once the solution of the first ‘‘hyperbolic’’ substep in (2.3) is computed, the intermediate cell averages,

$$\bar{\theta}_{j,k}^* \approx \frac{1}{\Delta x \Delta y} \iint_{C_{j,k}} \mathcal{S}_{\mathcal{H}}(\Delta t/2) \theta(x, y, t) dx dy,$$

become available. These data are then used as an initial condition for the parabolic IBVP:

$$\theta_t = \kappa \Delta \theta + s(x, y), \quad \theta(x, y, t) = \theta^*(x, y), \quad \theta \text{ is } (L, L)\text{-periodic}, \quad (2.13)$$

which is solved on the time interval  $(t, t + \Delta t]$  according to the Strang splitting algorithm (2.3). This can be done efficiently and with the exponential accuracy by the pseudo-spectral method. In our simulations, we first use the FFT algorithm to compute the discrete Fourier coefficients  $\hat{\theta}_{mn}(t)$  from the available point values  $\theta_{j,k}^*$  (notice that for finite-volume method of order less or equal to 2, the point values  $\theta_{j,k}^* \approx \bar{\theta}_{j,k}^*$ ) and approximate the solution at time  $t$  by

$$\theta(x, y, t) \approx \sum_{m,n} \hat{\theta}_{mn}(t) e^{\frac{2\pi(mx+ny)}{L}i}. \quad (2.14)$$

We then calculate the Fourier coefficients  $\hat{s}_{mn}$  of the source function  $s$  (this can be done even when  $s$  is singular, see Examples 2 and 3 in §3) and substitute them together with (2.14) into (2.13) to obtain simple linear ODEs for the discrete Fourier coefficients of  $\theta$ :

$$\frac{d}{dt} \hat{\theta}_{mn}(t) = -\kappa \frac{4\pi^2}{L^2} (m^2 + n^2) \hat{\theta}_{mn}(t) + \hat{s}_{mn}. \quad (2.15)$$

The last equation is solved exactly so that

$$\hat{\theta}_{mn}(t + \Delta t) = \hat{\theta}_{mn}(t) e^{-\alpha_{mn} \kappa \Delta t} + \hat{s}_{mn} \frac{1 - e^{-\alpha_{mn} \kappa \Delta t}}{\alpha_{mn} \kappa}, \quad \alpha_{mn} = \frac{4\pi^2(m^2 + n^2)}{L^2},$$

when  $m^2 + n^2 \neq 0$  and

$$\hat{\theta}_{00}(t + \Delta t) = \hat{\theta}_{00}(t) \equiv 0.$$

The latter is true since both  $\theta$  and  $s$  are spatially mean-zero quantities (see (1.3)). Finally, we use the inverse FFT algorithm to obtain the point values (and thus, the cell averages) of the solution at the new time level out of the set of the discrete Fourier coefficients,  $\{\widehat{\theta}_{mn}(t + \Delta t)\}$ . The obtained cell averages are denoted by  $\{\bar{\theta}_{j,k}^{**}\}$ .

The third (and last) substep of the Strang operator splitting (2.3) is again “hyperbolic”. We start with the cell averages  $\bar{\theta}_{j,k}^{**}$ , reconstruct a piecewise linear interpolant  $\widetilde{\theta}^{**}$  (following (2.5)–(2.7)), and then evolve it using the central-upwind scheme (2.8) as in the first “hyperbolic” substep to obtain the cell averages of the solution of (2.4) at the new time level  $t + \Delta t$ :

$$\bar{\theta}_{j,k}(t + \Delta t) \approx \frac{1}{\Delta x \Delta y} \iint_{C_{j,k}} \mathcal{S}_{\mathcal{H}}(\Delta t/2) \widetilde{\theta}^{**}(x, y) dx dy.$$

This completes the one time step description of the fast explicit operator splitting method.

### 3 Numerical Experiments

We consider the IBVP (2.4) on the square domain  $[0, L] \times [0, L]$ . We use the “random sine flow” that switches between

$$(u, v) = (\sqrt{2} U \sin[2\pi y/L + \phi], 0) \tag{3.1}$$

and

$$(u, v) = (0, \sqrt{2} U \sin[2\pi x/L + \phi]) \tag{3.2}$$

at time intervals of length  $1/2$ . The phase  $\phi$  is chosen randomly and uniformly from the interval  $[0, 2\pi)$  at each switch. This “toy” model of turbulence shares the basic properties of statistical homogeneity and isotropy with more sophisticated turbulent flows, and is often employed in studies of mixing. The coefficient  $\kappa$  is in the range  $10^{-5} - 10^{-1}$ . In the reported numerical tests we set the initial scalar concentration:

$$\Theta_0(x, y) = 0. \tag{3.3}$$

We would like to emphasize that the studied flow is in a highly turbulent regime (especially for small values of  $\kappa$ ), in which the solution is unstable and the only quantities that can be computed are the dimensionless *multi-scale mixing enhancement factors* introduced in [28]. More precisely, these time-space averaged quantities, denoted by  $\mathcal{E}_p$  for  $p \in \{-1, 0, 1\}$ , are defined as

$$\mathcal{E}_p^2 := \frac{\langle |\nabla^p \theta_s|^2 \rangle}{\langle |\nabla^p \theta|^2 \rangle}, \tag{3.4}$$

where  $\theta_s$  is the steady solution of the corresponding boundary-value problem:

$$\Delta \theta_s = -\frac{1}{\kappa} s(x, y), \quad \theta_s \text{ is } (L, L)\text{-periodic.}$$

The brackets  $\langle \cdot \rangle$  stand for the time-space average and are computed in terms of the Fourier coefficients of  $\theta$  ( $\theta_s$ ), such that

$$\langle |\nabla^p \theta|^2 \rangle = \sum_{m^2+n^2 \neq 0} \left[ \frac{4\pi^2}{L^2} (m^2 + n^2) \right]^p \overline{|\widehat{\theta}_{mn}|^2},$$

where

$$\widehat{\theta}_{mn}(t) = \int_0^1 \int_0^1 \theta(x, y, t) e^{-\frac{2\pi(mx+ny)}{L}i} dx dy \quad \text{and} \quad \overline{|\widehat{\theta}_{mn}|^2} = \lim_{t \rightarrow \infty} \frac{1}{t} \int_0^t |\widehat{\theta}_{mn}(\tau)|^2 d\tau.$$

These factors measure the effectiveness of stirring to suppress scalar fluctuations as a space-time averaged variance weighted at various scales. Stirring tends to enhance diffusive mixing and  $\mathcal{E}_p$  can also be considered as the diffusion “renormalization” factors in the following sense: if we define  $\kappa_p^{\text{effective}}$  as a value of molecular diffusion necessary to achieve the same scalar variance for  $p = 0$  without stirring (or gradient/inverse gradient variance for  $p = \pm 1$  respectively) as it is realized with stirring, when  $\kappa_p^{\text{effective}} = \kappa \mathcal{E}_p$ .

Unfortunately, the mixing enhancement factors  $\mathcal{E}_p$  cannot be computed exactly. However, the studied incompressible stirring flow field (3.1), (3.2) is statistically stationary, homogeneous and isotropic. In such a case, the following analytical upper bounds can be obtained, [6, 28]:

$$\mathcal{E}_1^2 \leq \frac{\sum_{m^2+n^2 \neq 0} \frac{|\widehat{s}_{mn}|^2}{m^2+n^2}}{\sum_{m^2+n^2 \neq 0} \frac{|\widehat{s}_{mn}|^2}{m^2+n^2 + U^2 L^2 / (2\pi\kappa)^2}}, \quad (3.5)$$

$$\mathcal{E}_0^2 \leq \frac{\sum_{m^2+n^2 \neq 0} \frac{|\widehat{s}_{mn}|^2}{(m^2+n^2)^2}}{\sum_{m^2+n^2 \neq 0} \frac{|\widehat{s}_{mn}|^2}{(m^2+n^2)^2 + (m^2+n^2)U^2 L^2 / (2\sqrt{2}\pi\kappa)^2}}, \quad (3.6)$$

$$\mathcal{E}_{-1}^2 \leq \frac{\sum_{m^2+n^2 \neq 0} \frac{|\widehat{s}_{mn}|^2}{(m^2+n^2)^3}}{\sum_{m^2+n^2 \neq 0} \frac{|\widehat{s}_{mn}|^2}{(m^2+n^2)^3 + (m^2+n^2)^2 U^2 L^2 / (2\sqrt{2}\pi\kappa)^2 + (m^2+n^2)\Omega^2 L^4 / (4\sqrt{2}\pi^2\kappa)^2}}. \quad (3.7)$$

Here  $\widehat{s}_{mn}$  are the Fourier coefficients of the source,  $U^2 = \langle |\mathbf{u}|^2 \rangle$  is the mean square velocity, and  $\Omega^2 = \langle \omega^2 \rangle$  is the enstrophy, the mean square vorticity ( $\omega = u_y - v_x$  is the vorticity).

These estimates suggest that the mixing efficiency of a flow may depend on the structure of the source-sink distribution that the flow is tasked to stir. In fact, this runs counter to the conventional notion of an effective diffusion or “eddy” diffusion determined solely by the flow. So it is interesting to study the observed source-dependence of these quantities to determine in which extent the qualitative prediction is realized in practice.

In the following numerical examples, we consider IBVP (2.4),(3.1)–(3.3) with different source-sink distributions  $s$  and compute the mixing enhancement factors  $\mathcal{E}_p$  by the fast explicit operator splitting method. We use different spatial grids to compute  $\mathcal{E}_p$  in (3.4), depending on the value of the Péclet number  $Pe = UL/\kappa$ , as it is summarized in Table 3.1 (we set  $U = L = 1$ ).

$Pe = UL/\kappa$	$10^1$	$10^2$	$10^3$	$10^4$	$10^5$
Grid Size	$64 \times 64$	$64 \times 64$	$128 \times 128$	$256 \times 256$	$512 \times 512$

Table 3.1: Spatial grids used in the numerical examples depending on the value of  $Pe = UL/\kappa$ .

We would like to point out that the definition of the mixing enhancement factors (3.4) involves the limit as  $t \rightarrow \infty$  of the long time average

$$\Theta(t) = \frac{1}{t} \int_0^t |\widehat{\theta}_{mn}(\tau)|^2 d\tau. \tag{3.8}$$

In practice, however, this quantity can only be computed for a long but finite period of time. As it follows from our observations, the averages  $\Theta$  have numerically converged in all examples as time increased. The convergence was non-monotone, so we ran our simulations until the magnitude of the oscillations in  $\Theta$  became relatively small. Depending on the type of the source and/or the Péclet number, the reported values of the mixing enhancement factors  $\mathcal{E}_p$  are subject to 0.03% ÷ 1.5% errors.

In the numerical tests below, we compare the computed values of  $\mathcal{E}_p$  with the analytical upper bounds (3.5)–(3.7) and with the results obtained by the spectral method from [28] (Example 1) and the particle simulations from [25] (Examples 2 and 3). In Example 3, in which the delta-type source is considered, we also demonstrate the efficiency of the fast explicit operator method by comparing its performance with an unsplit finite-volume scheme applied to the (2.4),(3.1)–(3.3) directly.

### Example 1 — Smooth Single-Scale Source

We start with the example of the simplest case of the single-scale “monochromatic” source-sink distribution:

$$s(x, y) = \sqrt{2} \sin[2\pi(x + y)], \tag{3.9}$$

whose Fourier efficiencies,  $\widehat{s}_{mn}$  (required to perform the parabolic substep of the operator splitting method) are

$$\widehat{s}_{mn} = \begin{cases} i\sqrt{2}/2, & m = n = -1, \\ -i\sqrt{2}/2, & m = n = 1, \\ 0, & \text{otherwise.} \end{cases}$$

Even though  $s$  is smooth, the solution of the IBVP (2.4), (3.1)–(3.3), (3.9) is still unstable and the exact values of the mixing enhancement factors are unavailable. We compute these factors numerically and show (in Figure 3.1) the results obtained by the operator splitting method for  $\mathcal{E}_1$ ,  $\mathcal{E}_0$ , and  $\mathcal{E}_{-1}$  as functions of the Péclet number, each plotted along with the numerical results obtained in [28] by the spectral method. As one can observe, the results obtained by the two different numerical methods are in a very good agreement, which supports the accuracy of the proposed operator splitting method. However, we would like to point out that the spectral

method will no longer be applicable in the singular source cases considered in Examples 2 and 3 below.

In the same figure, we also plot the upper bounds for  $\mathcal{E}_1$ ,  $\mathcal{E}_0$ , and  $\mathcal{E}_{-1}$  given by (3.5)–(3.7):

$$\mathcal{E}_1^2 \leq 1 + \frac{Pe^2}{8\pi^2}, \quad \mathcal{E}_0^2 \leq 1 + \frac{Pe^2}{16\pi^2}, \quad \mathcal{E}_{-1}^2 \leq 1 + \frac{3Pe^2}{32\pi^2}.$$

As pointed out by Plasting and Young [26] (see also [28]), the upper bounds are actually saturated by another statistically stationary homogeneous and isotropic stirring scheme. Nevertheless, these numerical experiments demonstrate that the enhancement factors generally depend on scale. In fact, this flow is closer to the optimal source-sink mixing on the large length scales than on the intermediate or small scales. Indeed, the observed  $\mathcal{E}_{-1}$  is almost  $\sim Pe$  as it is limited by the bound.

In Figure 3.2, we place the snapshots of the scalar field  $\theta$ , computed by the operator splitting method at time  $t = 50$  on a  $128 \times 128$  spatial grid for  $Pe = 10, 1000$ , and on a  $512 \times 512$  grid for 100000. One can observe that when the molecular diffusion coefficient is reduced and all other parameters are being fixed, the smaller and smaller length scales appear in the scalar distribution, even though the source contributes directly at the largest scale only.

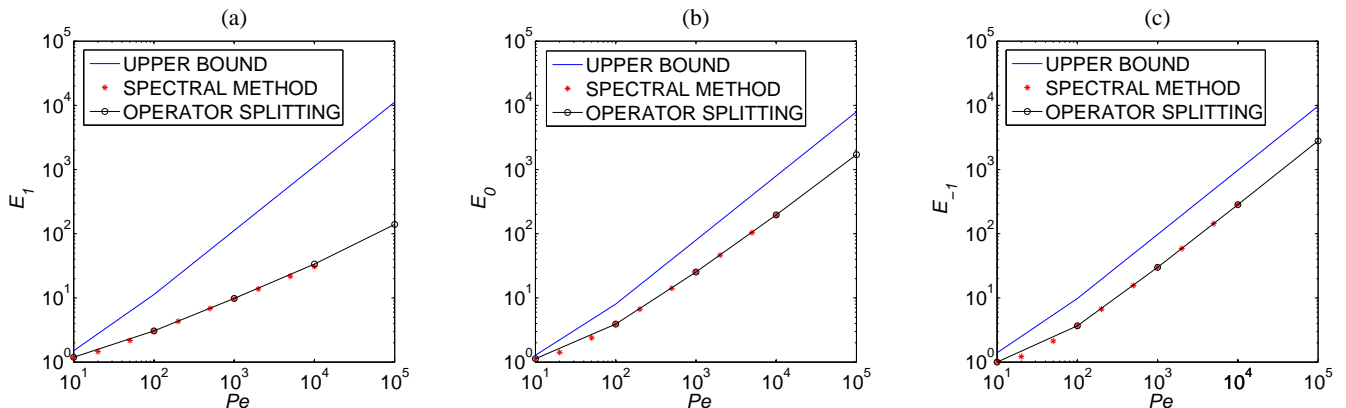


Figure 3.1: Mixing enhancement factors  $\mathcal{E}_p$  as a function of  $Pe$  for (a)  $p = 1$ , (b)  $p = 0$ , and (c)  $p = -1$  for the monochromatic source (3.9). The upper bounds are plotted along with the numerical approximations computed by the spectral and operator splitting methods.

### Example 2 — Discontinuous Square Sources

Next we consider a more difficult problem (taken from [25]) with the piecewise constant source:

$$s(x, y) = \begin{cases} 1, & \text{if } (x, y) \in [\frac{1}{2} - \frac{\varepsilon}{2}, \frac{1}{2} + \frac{\varepsilon}{2}] \times [\frac{1}{2} - \frac{\varepsilon}{2}, \frac{1}{2} + \frac{\varepsilon}{2}], \\ 0, & \text{otherwise,} \end{cases} \quad (3.10)$$

where  $\varepsilon$  is a small positive number.

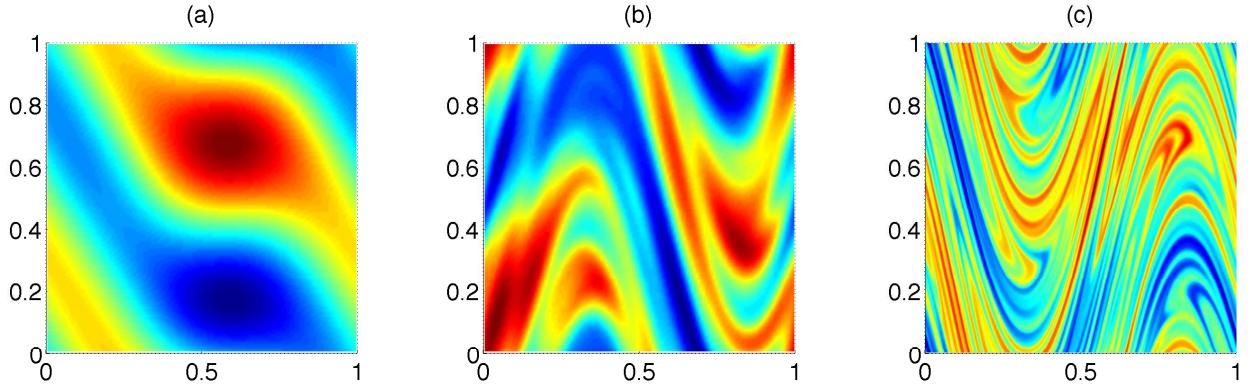


Figure 3.2: The scalar field stirred by the random sine flow for the source (3.9) with (a)  $Pe = 10$ , (b)  $Pe = 1000$ , computed on a  $128 \times 128$  grid, and (c)  $Pe = 100000$  computed on a  $512 \times 512$  grid.

We consequently reduce  $\varepsilon$  and set it equal to either  $1/2$ ,  $1/10$  or  $1/50$ . The Fourier coefficients,  $\widehat{s}_{mn}$ , of the source are given by

$$\widehat{s}_{mn} = \begin{cases} \frac{1}{mn\pi^2} \sin(\varepsilon m\pi) \sin(\varepsilon n\pi) e^{-i\pi(m+n)}, & m^2 + n^2 \neq 0, \\ \frac{\varepsilon}{n\pi} \sin(\varepsilon n\pi) e^{-i\pi n}, & m = 0, n \neq 0, \\ \frac{\varepsilon}{m\pi} \sin(\varepsilon m\pi) e^{-i\pi m}, & m \neq 0, n = 0, \\ 0, & \text{otherwise.} \end{cases}$$

In Figures 3.3(a), (b), and (c) we plot the enhancement factors  $\mathcal{E}_{-1}$ ,  $\mathcal{E}_0$ , and  $\mathcal{E}_1$ , respectively, computed by the operator splitting method as a function of the Péclet number. In Figure 3.4 we compare our results for  $\mathcal{E}_0$  with those obtained by the particle method in [25] for various values of  $\varepsilon$ . Again, one can observe a very good agreement between the results obtained by two different numerical methods. However, we would like to remind the reader (see also the discussion in §1) the limitations on both accuracy and efficiency of the particle method from [25] as well as the difficulty associated with its implementation. In addition, we note that no comparison of the mixing enhancement factors  $\mathcal{E}_1$  and  $\mathcal{E}_{-1}$  with the particle simulations has been provided since neither of these factors can be easily computed from the “pure” particle simulations.

### Example 3 — Singular Point Source

Finally, we take the  $\varepsilon = 0$  limit in the square size in (3.10), which corresponds to the singular point source

$$s(x, y) = \delta(x)\delta(y) - 1, \tag{3.11}$$

where  $\delta$  is the Dirac delta-function. The Fourier coefficients in this case are

$$\widehat{s}_{mn} = \begin{cases} e^{-i\pi(m+n)}, & m^2 + n^2 \neq 0, \\ 0, & \text{otherwise.} \end{cases}$$

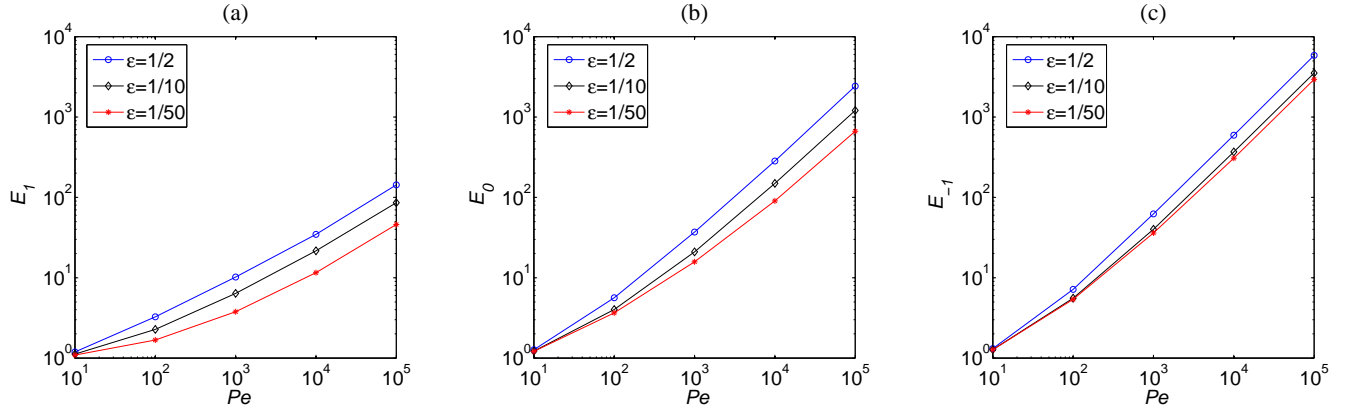


Figure 3.3: Mixing enhancement factors  $\mathcal{E}_p$  as a function of  $Pe$  for (a)  $p = 1$ , (b)  $p = 0$ , and (c)  $p = -1$  for the shrinking square sources (3.10).

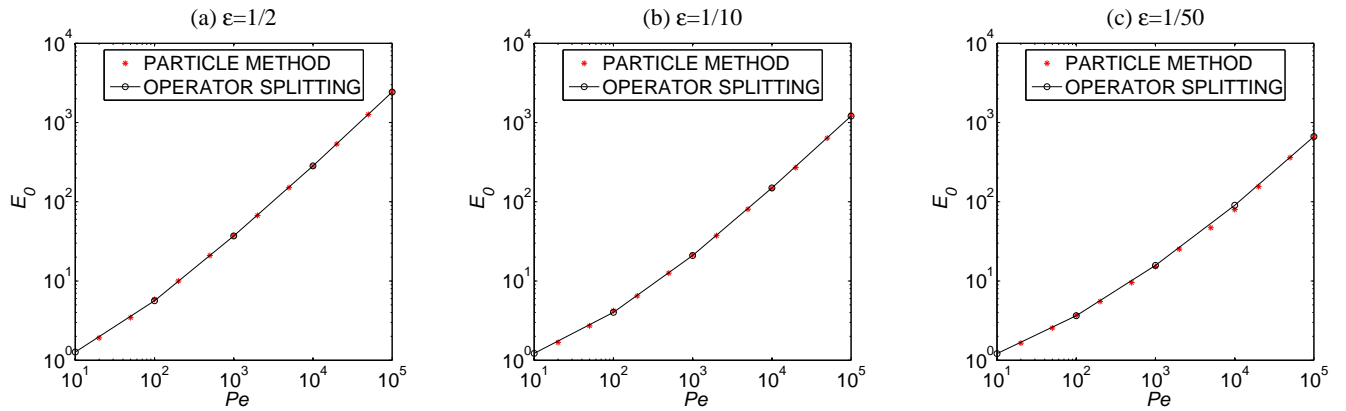


Figure 3.4: The computed factors  $\mathcal{E}_0$  are compared to that obtained by the particle method from [25] for (a)  $\varepsilon = 1/2$ , (b)  $\varepsilon = 1/10$ , and (c)  $\varepsilon = 1/50$ .

This is the most challenging numerical example. Here we compare the numerical results obtained by the fast explicit operator splitting method with the particle method simulations. In Figure 3.5 we plot the enhancement factors  $\mathcal{E}_0$  and  $\mathcal{E}_{-1}$  computed by the operator splitting method and the corresponding analytical upper bounds as functions of  $Pe$  obtained from (3.6)–(3.7). For this singular source the gradient variance is infinite and the upper bound (3.5) on  $\mathcal{E}_1 = 1$ . In Figure 3.5(a), we also compare the mixing enhancement factors  $\mathcal{E}_0$  computed by the operator splitting method with those obtained by the particle method in [25] (no particle results are shown in Figure 3.5(b), since the values of  $\mathcal{E}_{-1}$  cannot be obtained from the particle simulation). Again, both computations are in a very good agreement, especially for small Péclet numbers, but the same issues related to the accuracy, efficiency and the practical implementation of the particle method, which have been discussed in §1 and Example 2, are also relevant here.

In addition, we demonstrate the efficiency of the fast explicit operator splitting method by comparing its performance with the performance of an unsplit finite-volume method. In the latter method, the cell averages of  $\theta$  are evolved in time by solving the following system of

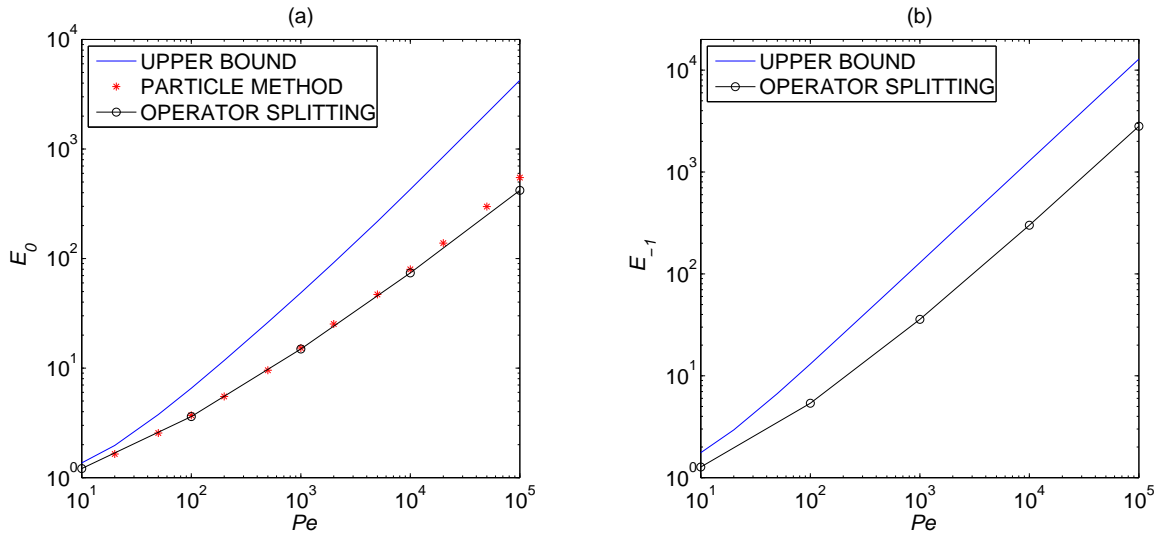


Figure 3.5: Mixing enhancement factors  $\mathcal{E}_0$  and  $\mathcal{E}_{-1}$  as a function of  $Pe$  for the singular source (3.11).

time-dependent ODEs:

$$\begin{aligned} \frac{d}{dt} \bar{\theta}_{j,k}(t) = & - \frac{H_{j+\frac{1}{2},k}^x(t) - H_{j-\frac{1}{2},k}^x(t)}{\Delta x} - \frac{H_{j,k+\frac{1}{2}}^y(t) - H_{j,k-\frac{1}{2}}^y(t)}{\Delta y} \\ & + \kappa \left[ \frac{\bar{\theta}_{j+1,k}(t) - 2\bar{\theta}_{j,k}(t) + \bar{\theta}_{j-1,k}(t)}{(\Delta x)^2} + \frac{\bar{\theta}_{j,k+1}(t) - 2\bar{\theta}_{j,k}(t) + \bar{\theta}_{j,k-1}(t)}{(\Delta y)^2} \right] + \bar{s}_{j,k}, \end{aligned} \quad (3.12)$$

where  $H_{j+\frac{1}{2},k}^x(t)$  and  $H_{j,k+\frac{1}{2}}^y(t)$  are the central-upwind numerical fluxes given by (2.9) and

$$\bar{s}_{j,k} = \begin{cases} -1 + \frac{1}{\Delta x \Delta y}, & \text{if } x_j = y_k = 1/2, \\ -1, & \text{otherwise.} \end{cases}$$

The ODE system (3.12) is very stiff. Hence it should be integrated by an efficient ODE solver. In this example, we have used the explicit third-order large stability domain Runge-Kutta method, developed in [22,23]. This high-order integration produces accurate results, and its larger stability domains (in comparison with the standard Runge-Kutta methods) allow one to use larger time steps; the explicit form retains simplicity, and the embedded formulas permit an efficient stepsize control. In practice these methods preserve all the advantages of explicit methods and work as fast as implicit methods (see [23] for details).

In Table 3.2, we compare the CPU times required to perform the calculations by both the *fast explicit operator splitting* and the *unsplit finite-volume* methods until time  $t = 2000$ , when the integral (3.8) converges to the same accuracy. As one see, the fast explicit operator splitting method is much faster than the unsplit finite-volume one.

## 4 Summary and Conclusions

We have applied the fast explicit operator splitting framework to the mixing enhancement problem described by an advection-diffusion equation with a temporally random velocity field and a

$Pe = UL/\kappa$	$10^1$	$10^2$	$10^3$	$10^4$
Splitting	8	8	75	746
No Splitting	49	20	168	3196

Table 3.2: CPU times (in minutes) compared for different values of  $Pe = UL/\kappa$ .

singular source. In the proposed splitting approach, the hyperbolic and parabolic subproblems have been solved by two different methods: The hyperbolic equation has been solved numerically by the second-order Godunov-type central-upwind scheme while the parabolic equation has been solved exactly using the pseudo-spectral technique. The combined method has been tested on three numerical examples with various parameters and the results have been compared with those obtained by the spectral and particle methods. We have demonstrated that all numerical methods tested in this work yield comparable results while applied to the model problems. However, the fast explicit operator splitting method has a number of advantages over other discussed methods:

- The major advantage of the proposed technique compared to the spectral approach is its ability to handle singular point-sources — a most interesting and challenging problem from the practical point of view;
- The accuracy of the particle code is limited by the finite number of particles that can be tracked, which, in turn, leads to both the statistical and the systematic errors and the necessity to implement a procedure that constantly adds and removes particle during numerical simulations (see the discussion in [25]). On the other hand, the operator splitting method has much better convergence properties, especially in the convection dominated regime ( $\kappa \ll 1$ ). In addition, the operator splitting approach allows us a straightforward computation of the inverse gradient variance for a large scale mixing enhancement;
- Finally, the most important benefit in using the fast explicit operator splitting method is its simplicity, efficiency and applicability to a more general class of problems, for example, to the models in which the stirring velocity field is a turbulent solution of the incompressible Navier-Stokes equation. The latter is of significant interest and will be studied in our future work.

**Acknowledgment:** This research was supported in parts by US National Science Foundation Grants DMS-0410023 (AC), PHY-0555324 and DMS-0553487 (CRD), DMS-0610430 (AK), and DMS-0712898 (AC). One of us (CRD) is especially grateful for the hospitality of the Institute for Pure & Applied Mathematics at UCLA and the Geophysical Fluid Dynamics Program at Woods Hole Oceanographic Institution where parts of this work was completed.

## References

- [1] A. CHERTOCK, E. KASHDAN, AND A. KURGANOV, *Propagation of diffusing pollutant by a hybrid Eulerian-Lagrangian method*, in Hyperbolic problems: theory, numerics, applications (Lyon 2006), S. Benzoni-Gavage and D. Serre, eds., Springer, 2008, pp. 371–380.

- [2] A. CHERTOCK AND A. KURGANOV, *On splitting-based numerical methods for convection-diffusion equations*, in Numerical Methods for Balance Laws, G. Puppo and G. Russo, eds., Quaderni di Matematica. To appear.
- [3] A. CHERTOCK, A. KURGANOV, AND G. PETROVA, *Fast explicit operator splitting method. Application to the polymer system*, in Finite Volumes for Complex Applications IV, F. Benkhaldoun, D. Ouazar, and S. Raghu, eds., Hermes Science, 2005, pp. 63–72.
- [4] A. CHERTOCK, A. KURGANOV, AND G. PETROVA, *Fast explicit operator splitting method for convection-diffusion equations*, Internat. J. Numer. Meth. Fluids, 59 (2009), pp. 309–332.
- [5] B. COCKBURN, C. JOHNSON, C.-W. SHU, AND E. TADMOR, *Advanced numerical approximation of nonlinear hyperbolic equations*, in CIME Lecture Notes, A. Quarteroni, ed., vol. 1697 of Lecture Notes in Mathematics, Springer-Verlag, 1997.
- [6] C.R. DOERING AND J.-L. THIFFEAULT, *Multiscale mixing efficiencies for steady sources*, Phys. Rev. E., 74, 025301(R) (2006).
- [7] I. T. DRUMMOND, *Path-integral methods for turbulent diffusion*, J. Fluid Mech., 123 (1982), pp. 59–68.
- [8] E. GODLEWSKI AND P.-A. RAVIART, *Numerical approximation of hyperbolic systems of conservation laws*, vol. 118 of Applied Mathematical Sciences, Springer-Verlag, New York, 1996.
- [9] S. GOTTLIEB, C.-W. SHU, AND E. TADMOR, *Strong stability-preserving high-order time discretization methods*, SIAM Rev., 43 (2001), pp. 89–112.
- [10] W. HUNSDORFER AND J. VERWER, *Numerical solution of time-dependent advection-diffusion-reaction equations*, vol. 33 of Springer Series in Computational Mathematics, Springer-Verlag, Berlin, 2003.
- [11] D. KRÖNER, *Numerical schemes for conservation laws*, Wiley-Teubner Series Advances in Numerical Mathematics, John Wiley & Sons Ltd., Chichester, 1997.
- [12] A. KURGANOV AND C.-T. LIN, *On the reduction of numerical dissipation in central-upwind schemes*, Commun. Comput. Phys., 2 (2007), pp. 141–163.
- [13] A. KURGANOV, S. NOELLE, AND G. PETROVA, *Semi-discrete central-upwind scheme for hyperbolic conservation laws and Hamilton-Jacobi equations*, SIAM J. Sci. Comput., 23 (2001), pp. 707–740.
- [14] A. KURGANOV AND E. TADMOR, *New high resolution central schemes for nonlinear conservation laws and convection-diffusion equations*, J. Comput. Phys., 160 (2000), pp. 241–282.
- [15] A. KURGANOV AND E. TADMOR, *Solution of two-dimensional Riemann problems for gas dynamics without Riemann problem solvers*, Numer. Methods Partial Differential Equations, 18 (2002), pp. 584–608.

- [16] J. LEE AND B. FORNBERG, *A split step approach for the 3-D Maxwell's equations*, J. Comput. Appl. Math., 158 (2003), pp. 485–505.
- [17] R.J. LEVEQUE, *Finite volume methods for hyperbolic problems*, Cambridge Texts in Applied Mathematics, Cambridge University Press, Cambridge, 2002.
- [18] K.-A. LIE AND S. NOELLE, *On the artificial compression method for second-order nonoscillatory central difference schemes for systems of conservation laws*, SIAM J. Sci. Comput., 24 (2003), pp. 1157–1174.
- [19] A. J. MAJDA AND P. R. KRAMER, *Simplified models for turbulent diffusion: theory, numerical modelling, and physical phenomena*, Phys. Rep., 314 (1999), pp. 237–574.
- [20] G.I MARCHUK, *Metody rasshchepleniya*, (Russian) [Splitting Methods] “Nauka”, Moscow, 1988.
- [21] G.I MARCHUK, *Splitting and alternating direction methods*, in Handbook of numerical analysis, Vol. I, Handb. Numer. Anal., I, North-Holland, Amsterdam, 1990, pp. 197–462.
- [22] A.A. MEDOVIKOV, DUMKA 3 code available at <http://www.math.tulane.edu/~amedovik/>.
- [23] A.A. MEDOVIKOV, *High order explicit methods for parabolic equations*, BIT, 38 (1998), pp. 372–390.
- [24] H. NESSYAHU AND E. TADMOR, *Nonoscillatory central differencing for hyperbolic conservation laws*, J. Comput. Phys., 87 (1990), pp. 408–463.
- [25] T. OKABE, B. ECKHARDT, J.-L. THIFFEAULT, AND C.R. DOERING, *Mixing effectiveness depends on the source-sink structure: Simulation results*, J. Stat. Mech. Theory Exp., P07018 (2008), pp. 1–13.
- [26] S. C. PLASTING AND W. R. YOUNG, *A bound on scalar variance for the advection-diffusion equation*, J. Fluid Mech., 552 (2006), pp. 289–298.
- [27] G. RUSSO, *Central schemes and systems of balance laws*, in Hyperbolic partial differential equations (Hamburg, 2001), Vieweg, Braunschweig, 2002, pp. 59–114.
- [28] T.A. SHAW, J.-L. THIFFEAULT, AND C.R. DOERING, *Stirring up trouble: multi-scale mixing measures for steady scalar sources*, Phys. D, 231 (2007), pp. 143–164.
- [29] G. STRANG, *On the construction and comparison of difference schemes*, SIAM J. Numer. Anal., 5 (1968), pp. 506–517.
- [30] P.K. SWEBY, *High resolution schemes using flux limiters for hyperbolic conservation laws*, SIAM J. Numer. Anal., 21 (1984), pp. 995–1011.
- [31] H. YOSHIDA, *Construction of higher order symplectic integrators*, Phys. Lett. A, 150 (1990), pp. 262–268.